scientific reports

Check for updates

OPEN

Investigation of nozzle angle on the microstructure and abrasion resistance of jet electrodeposited Ni-TiC composites

Mengyu Cao[1,4], Dehao Tian[1], Chaoyu Li[2,4]✉, BaoJin Wang[1]✉, Xue Guo[1]✉, Wei Li[3]✉ & Fengwu Zhang[2]

In order to study nozzle angle on the abrasion resistance of nickel-titanium carbide (Ni-TiC) composites, the jet electrodeposited Ni-TiC composite coating was fabricated at nozzle angles of 30°, 45° and 60°. The jet velocity and kinetic energy of the electrolyte at different nozzle angles within the given range of 30°–60° were simulated by means of COMSOL software. Additionally, the surface morphology, phase structure, and abrasion resistance of the Ni-TiC composites prepared at various jet angles were investigated using a scanning electron microscopy, energy dispersive spectroscopy, X-ray diffraction analysis, and a friction-abrasion testing machine, respectively. The simulation results indicated that at a nozzle angle of 45°, the jet speed and spraying pressure of the electrolyte were 3.17 m/s and 3.18 × 10⁴ Pa, respectively. The Ni-TiC composites fabricated at nozzle angle of 45° had dense and smooth surface morphology with uniform distribution of TiC nanoparticles. Furthermore, at this nozzle angle, the composite demonstrated the smallest nanoparticle size (60.8 nm) and the highest TiC content (4.82 wt%). These findings confirm that the nozzle angle plays a crucial role in the distribution and incorporation of TiC nanoparticles, directly influencing the abrasion resistance of the composite. Notably, the Ni-TiC composite deposited at 45° exhibited the lowest friction coefficient and minimal mass loss, confirming its superior abrasion resistance.

Keywords Ni-TiC composites, Jet electrodeposition, Nozzle angle, Microstructure, Abrasion performance

Nickel is commonly employed as the primary constituent in coatings designed for enhancing the corrosion resistance and wear durability of critical components. Nonetheless, with the escalating demands in sectors such as aerospace, automotive, and shipbuilding, conventional pure nickel coatings have fallen short of meeting the rigorous performance benchmarks[1–3]. Consequently, the incorporation of nanoparticles (NPs) such as silicon carbide (SiC), alumina (Al_2O_3), titanium nitride (TiN), and diamond into pure nickel has been extensively studied to enhance its chemical and physical properties, thereby broadening the application scope of these advanced materials[4–6]. Nyambura et al.[7] synthesized Ni-W and Ni-W/Cr_2O_3 composites utilizing an electrodeposition approach. They reported that the Ni-W/Cr_2O_3 composites demonstrated significantly enhanced microhardness and corrosion resistance compared to the base Ni-W alloy. Shao et al.[8] employed the electrodeposition technique to fabricate pure Ni coatings and Ni-TiO_2 composite coatings. They observed that the pure Ni coatings exhibited significantly inferior wear and corrosion resistance compared to the Ni-SiC composite coatings. Qu et al.[9] employed the electrodeposition technique to fabricate composite coatings and found that the Ni-CeO_2 composite coatings demonstrated significantly enhanced wear resistance in comparison to pure Ni coatings. Furthermore, they observed a strong correlation between the CeO_2 content and the wear resistance of theNi-CeO_2 composites. These studies concluded that the incorporation of NPs into a nickel matrix, prepared via the electrodeposition method, significantly enhanced the properties of the resulting composites.

The microstructure and properties of metallic composites are significantly influenced by operation parameters and processing approach[10,11]. Consequently, numerous researchers worldwide have embarked on diverse endeavors aimed at enhancing the properties of metallic composite. For instance, Fu et al.[12] optimized

[1]School of Mechanical Science and Engineering, Northeast Petroleum University, Daqing 163318, China. [2]School of Mechanical and Electrical Engineering, Sanming University, Sanming 365004, China. [3]School of Petroleum Engineering, Northeast Petroleum University, Daqing 163318, China. [4]Mengyu Cao and Chaoyu Li contributed equally to this work. ✉email: dotalcy@163.com; bjwangbaojin@nepu.edu.cn; GX_CMY@nepu.edu.cn; liwei@nepu.edu.cn

the mechanical properties of metallic alloy by combining directed energy deposition (DED) and layer by layer ultrasonic shock peening (UDED) techniques, and introducing electric pulse treatment (EPT). The study concluded that the correlation between electric pulse treatment and microstructure evolution, providing a new method for customized control of the mechanical properties of metallic alloy. Gyawali et al.[13] investigated the influence of ultrasonic frequency and power on the anti-wear and anti-corrosion properties of Ni-SiC coatings fabricated through electrochemical methods. Their findings demonstrated that the incorporation of ultrasonic waves significantly enhanced the abrasion and corrosion resistance of the Ni-SiC coating. Yang et al.[14] studied the process and properties of preparing nitrogen doped CoCrFeNiMn high entropy alloy coating (N-HEA) on alloy surface using high-speed oxygen fuel spraying (HVOF) combined with dual glow plasma nitriding technology. Their results revealed the microhardness and abrasion resistance of metallic composites were significantly improved using compound process, providing new idea for surface modification of alloys. Hu et al.[15] explored the influence of electrode rotation speed on the corrosion resistance of Ni-Co coatings fabricated via electrodeposition. They observed that rotating the cathode effectively mitigated hydrogen bubble adsorption on the surface. Jet electrodeposition (JE) stands as a quintessential surface processing technique, renowned for its facile operation, remarkable efficiency, and economic viability. It constitutes a pivotal strategy in the fabrication of protective surface coatings[16]. Furthermore, TiC NPs are extensively utilized to fabricate composites exhibiting exceptional abrasive resistance, attributed to their high microhardness, mature stability, and robust adhesion properties[17]. These findings underscored the parameter optimization and combination of various preparation approach contributed to enhance microstructure and abrasion resistance of metallic composites.

Nonetheless, prevailing literature predominantly centers on the operation parameters of the JE technique for synthesizing Ni-based composites. However, the study about microstructural characteristics and abrasion resistance of Ni-TiC composites fabricated at different nozzle angles were examined utilizing a scanning electron microscopy (SEM), X-ray diffraction (XRD), and comprehensive friction-wear testing is scant. In addition, the scope of this study, computational simulations employing COMSOL Multiphysics software were also conducted to analyse the jet velocity and kinetic energy characteristics of the electrolyte. The outcomes derived from both simulations and experimental characterizations serve to significantly advance the understanding of the deposition mechanisms and enhanced abrasion resistance of Ni-TiC composites. Moreover, the three-dimensional (3D) printing technology is introduced to prepare the nozzle with different angles. As a result, our study is essential and novel with a combination of electrodeposition and 3D printing technology, broadening the technological applications of Ni-TiC composites.

Experiment

Preparation

The A3 steel specimen, measuring 30*12*4 mm^3, was employed as the cathode. The anode configurations consisted of nozzles fabricated at varied angles of 30°, 45°, and 60° utilizing fused deposition modeling technology, each integrated with a nickel rod of 3 mm diameter serving as the anodic component. Before the JP experiment, the surface of the A3 steel substrate was meticulously polished using a TP502 polisher to achieve a surface roughness of 0.25 μm. Afterwards, the polished substrate was descaling, degreasing, and activated in order. Finally, the disposed substrate was rinsed with distilled water and placed on the insulating plate. Moreover, TiC NPs with an average size of 40 nm were acquired from Daqing Tongda Nanotechnology Co. Ltd. The corresponding TEM image and XRD pattern are depicted in Fig. 1. The diffraction peaks of the TiC nanoparticles (NPs) were observed at 2θ values of 36.1°, 41.8°, 60.3°, 72.5° and 76.1°, which correspond to the crystallographic planes (111), (200), (220), (311), and (222), respectively. Figure 2a presents the experimental

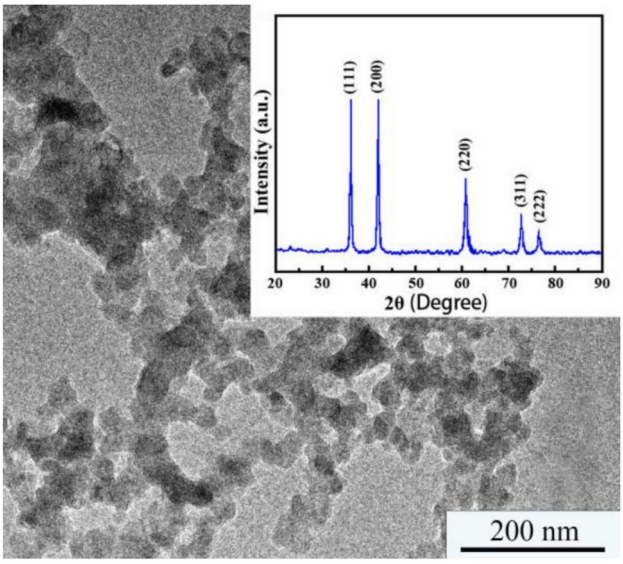

Fig. 1. TEM diagram and XRD pattern of TiC particles.

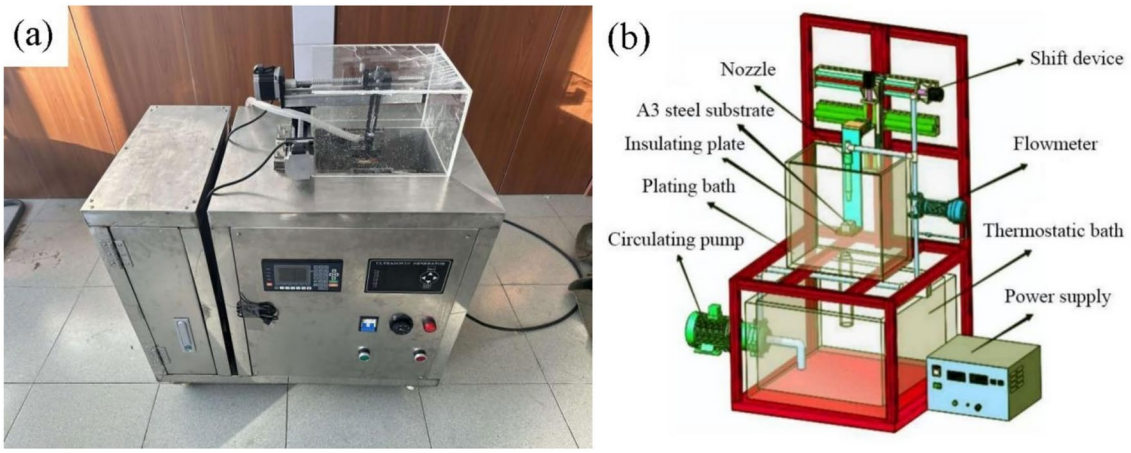

Fig. 2. (**a**) Experimental setup and (**b**) schematic diagram of the experimental apparatus.

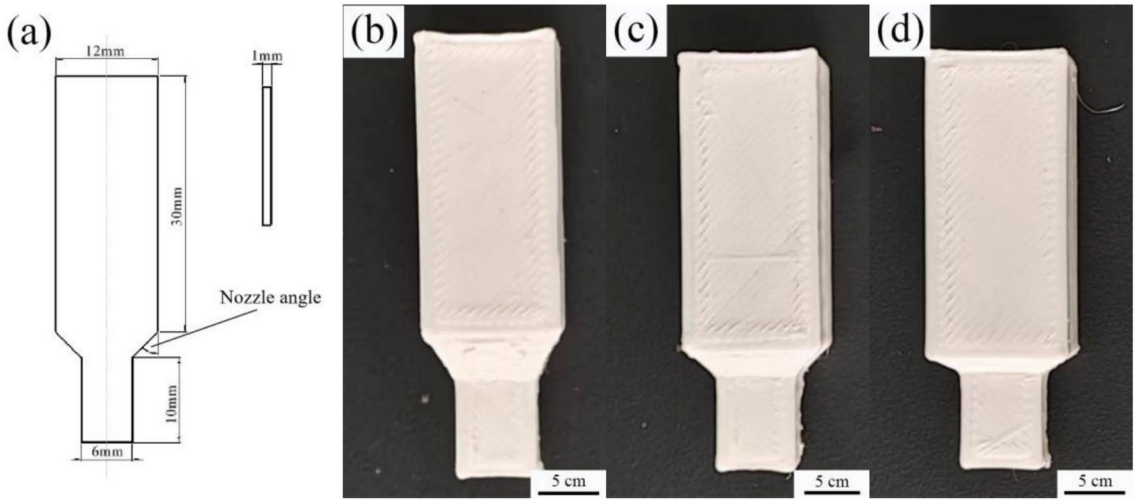

Fig. 3. (**a**) Specific size and experimental nozzle with different angles used for fabricating Ni-TiC composites: (**b**) 30°, (**c**) 45°, and (**d**) 60°

setup, and Fig. 2b illustrates the schematic diagram of the experimental apparatus employed for the synthesis of Ni-TiC composites via the jet electrodeposition (JE) technique. The schematic diagram of the experimental setup for synthesizing Ni-TiC composites via the jet electrodeposition (JE) technique is depicted in Fig. 2. This system is bifurcated into two principal components: the circulating flow part (including the thermostatic bath, flowmeter, shift device, nozzle, plating bath, and circulating pump) and the electrodeposition part (comprising the power supply, A3 steel substrate, and insulating plate). The specific dimensions and the experimental nozzles with different angles are presented in Fig. 3.

The SMD-100 type power supply was employed to deliver pulse current for the electroplating process. The pH of the electrolyte solution was precisely adjusted by employing hydrochloric acid and sodium hydroxide solutions, with respective molar concentrations of 4 mol/L and 2 mol/L. The inter-electrode distance was set to 20 mm. During electrodeposition process, the operation parameters and specific data of electrolyte are listed in Tables 1 and 2.

Characterization

During the JE process, a simulation of the jet speed and spraying pressure of the electrolyte was conducted using COMSOL software to fabricate Ni-TiC composites. The surface morphology of the Ni-TiC composites was examined using SEM (FEG 450) both before and after undergoing corrosion testing. The TiC content within the Ni-TiC composites was quantified utilizing energy dispersive spectroscopy (EDS). The phase constitution was identified using an X-ray diffractometer (XRD, model D5000) equipped with a Cu Kα target. The scan was conducted over a 2θ range of 20° to 80° with a step size of 0.01°. The nickel grain size (D) of the Ni-TiC composites was determined using Eq. (1):

Parameters	Specific
Current density	40 A/dm^2
pH value	4.3
Nozzle angle	30°,45°, 60°
Electrolyte temperature	55 °C
Plating time	40 min
Jet velocity	2 m/s

Table 1. Operation parameters of electrodeposited Ni-TiC composites.

Composition	Specific
TiC concentration	8 g/L
H_3BO_3	25 mg/L
$NiSO_4{\cdot}6H_2O$	210 g/L
$NiCl_2{\cdot}6H_2O$	35 g/L
Cetyl trimethyl ammonium bromide	40 mg/L

Table 2. Chemical reagent of electrolyte for preparing Ni-TiC composites.

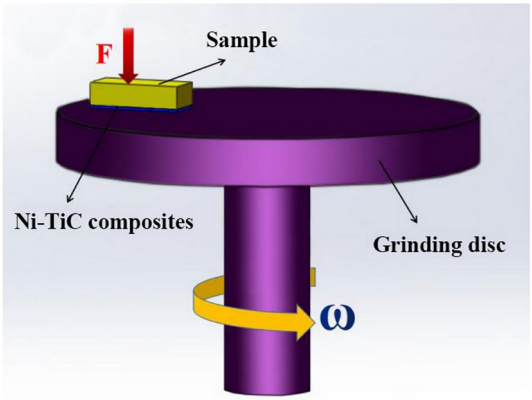

Fig. 4. Schematic illustration for measuring abrasion resistance of Ni-TiC composites.

$$D = \frac{K\gamma}{Bcos\theta} \tag{1}$$

where K represented the Scherrer constant (0.89), γ denoted the wavelength of X-rays (0.154056 nm), B was the full-width at half-maximum (FMHM) of the diffraction peak, and θ signified the Bragg angle.

The microhardness of the Ni-TiC composites was assessed using a Hv-1000 Vickers hardness tester. According to the ASTM standard, the five measured results from micro-hardness test of Ni-TiC composites are recorded and averaged. The testing parameters were set as follows: an applied load of 25 g and a dwell time of 10 s. The microhardness value (H) of the Ni-TiC composites was calculated using Eq. (2).

$$H = (1854.4 \times 10^6 \times 0.102F)/d^2 \tag{2}$$

where F was the applied load weight under vertical direction, and d was the diagonal length of indentation.

The abrasion resistance of the Ni-TiC composites was assessed using a HRS-2 M friction and wear tester. The schematic diagram illustrating the procedure for measuring the abrasion resistance of the Ni-TiC composites is presented in Fig. 4. The measurement conditions were the friction pair consisted of 40Cr hardened steel, with an applied loading force (F) of 5 N, rotational speed (ω) of 300r/min and a duration time of 15 min, respectively. The abrasion weight loss (W) of the composites was calculated using Eq. (3):

$$W = W_1 - W_2 \tag{3}$$

where W_1 and W_2 was the weight of composites before and after abrasion test, respectively.

Results and discussion

JE simulation analysis

The nozzle angle significantly influences the jet velocity and spraying pressure of the electrolyte during the JE process. Optimised jet speed and spraying pressure enhance TiC NP dispersion on the steel substrate. Meanwhile, the jet velocity and spraying pressure had apparent effect on the nucleation process and grain growth, leading to the microstructure and performances of nickel matrix composite coatings are varied dramatically[18]. Consequently, the jet speed and spraying pressure of the electrolyte were simulated utilizing COMSOL Multiphysics software. The simulated results for the jet velocity and spraying pressure of the electrolyte at various nozzle angles are depicted in Fig. 5. Specifically, Fig. 5a–c illustrates the simulated jet velocity of the electrolyte during the JE process, while Fig. 5a'–c' displays the corresponding simulated electrolyte spraying pressure throughout the JE process.

The simulation results revealed that the jet velocity and spraying pressure of the electrolyte reached their minimum values at a nozzle angle of 30°, with the jet velocity being 2.81 m/s and the spraying pressure measuring 3.04×10^4 Pa. In contrast, the simulation results indicated that both the jet velocity and the spraying pressure of the electrolyte exhibited an increase at a nozzle angle of 45°, with the former increasing by 12.8% to 3.17 m/s and the latter rising by 4.6% to 3.18×10^4 Pa. Upon increasing the nozzle angle from 45° to 60°, the simulation results demonstrated a rise in both the jet velocity and the spraying pressure of the electrolyte, increasing by 7.9% to 3.42 m/s and rising 3.8% to 3.3×10^4 Pa, respectively. The simulation results of the JE process revealed that both the jet velocity and spraying pressure of the electrolyte exhibited an increase as the nozzle angle was varied from 30° to 60°.

SEM images investigation

Figure 6 presents SEM images of Ni-TiC composites fabricated at different nozzle angles. As depicted, the coarse and large nickel grains emerged on the surface morphology of the Ni-TiC composite prepared at a nozzle angle of 30°. By contrast, the composite fabricated at a nozzle angle of 45° displays a compact and flattened surface morphology characterized by refined nickel grains. However, further increasing the nozzle angle to 60°, the small pores appeared on the surface morphology of composites and the size of nickel grains became large again. Additionally, severe agglomeration of TiC NPs was observed on the surface of the composite fabricated at a 30° nozzle angle, whereas a uniform distribution of TiC NPs was evident on the surface of the composite fabricated at a 45° nozzle angle.

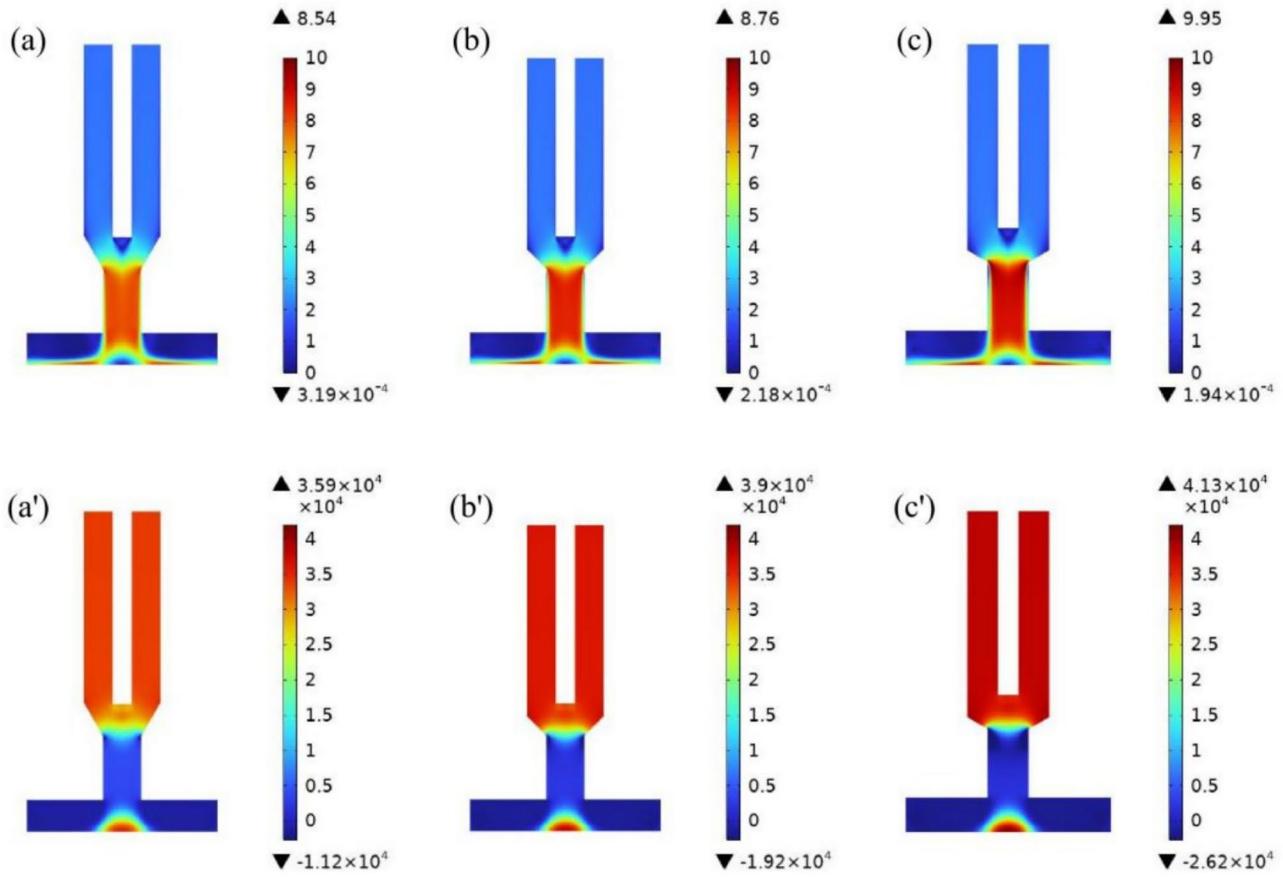

Fig. 5. Simulated images of (**a**)–(**c**) jet velocity and (**a'**)–(**c'**) spraying pressure of electrolyte obtained at different nozzle angles.

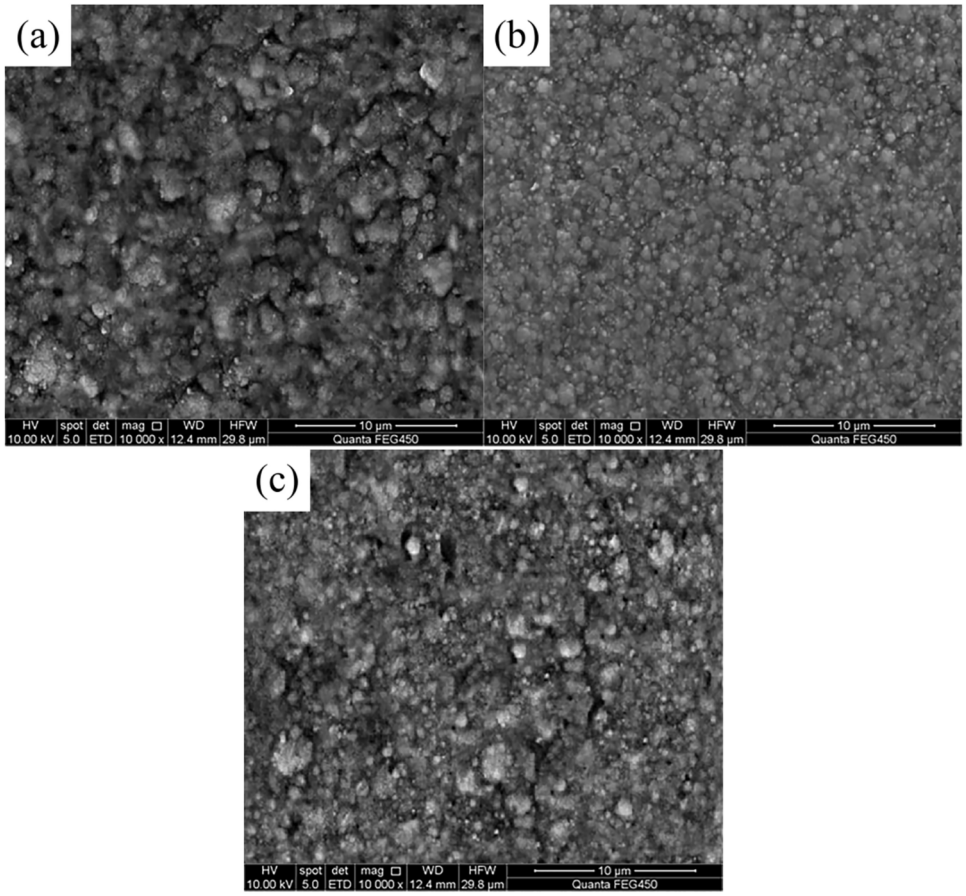

Fig. 6. SEM images of Ni-TiC composites manufactured at various nozzle angles: (**a**) 30°, (**b**) 45°, and (**c**) 60°

The surface morphology of Ni-TiC composites was obviously influenced by jet velocity and spraying pressure. This can be attributed to the fact that the low jet velocity and spraying pressure at nozzle angle of 30° had a low quantity of TiC NPs, leading to nucleation sites decreased and rapid growth of nickel grain suppressed[19]. The nozzle angle of 45° increased jet velocity and spraying pressure, reduced the thickness of the diffusion layer and enhanced co-deposition rate of Ni^{2+} ions and TiC NPs, resulting in the generation of strong fine-grain strengthening and surface morphology of composite became dense and smooth[20]. Conversely, the high jet speed and spraying pressure (nozzle angle of 60°) aggravated agglomeration of TiC NPs, leading to the number of nucleation point decreased and nickel grain size increased[21]. In addition, the high jet speed and spraying pressure unfavorable for growth of composites, resulting in small pore emerged on the composite surface.

TiC NPs measurement

Figure 7 illustrates the size distribution and content of TiC NPs within the three Ni-TiC composites, as determined by SEM imaging and EDS analysis. At a nozzle angle of 30°, the average diameter of TiC NPs in the Ni-TiC composite was approximately 95.3 nm, with the majority of particles ranging from 80 to 110 nm. In contrast, at an angle of 45° for the nozzle, the average particle size decreased significantly to 60.8 nm, predominantly concentrated between 50 and 80 nm. Meanwhile, at 60°, the mean TiC NP size increased to 76.4 nm, primarily within the 60–90 nm range. Additionally, the TiC NPs content in the Ni-TiC composites fabricated at nozzle angles of 30°, 45°, and 60° was found to be 2.65 wt%, 4.82 wt%, and 3.71 wt%, respectively.

Ren et al.[22] reported that the appropriate jet speed and spraying pressure could enhance the content and distribution of reinforced phase in the electrodeposited composites. This result could be explained that optimal nozzle angle facilitates the co-deposition rate of TiC NPs with Ni^{2+} ions and reduces agglomeration of TiC NPs[23]. By comparison, an high jet velocity and spraying pressure aggravate agglomeration of TiC particles and reduce TiC content in the composites[24].

XRD pattern observation

Figure 8 illustrates the XRD patterns of Ni-TiC composites fabricated at various nozzle angles. The XRD patterns reveal that both nickel and TiC phases are present in all three Ni-TiC composites, indicating that both TiC NPs and nickel grains contributed to the substrate formation. Additionally, the intensity of the nickel phase diffraction peaks initially decreases and then increases with increasing nozzle angle. According to Eq. (1), the average sizes of the nickel grains in the Ni-TiC composites fabricated at nozzle angles of 30°, 45°, and 60°

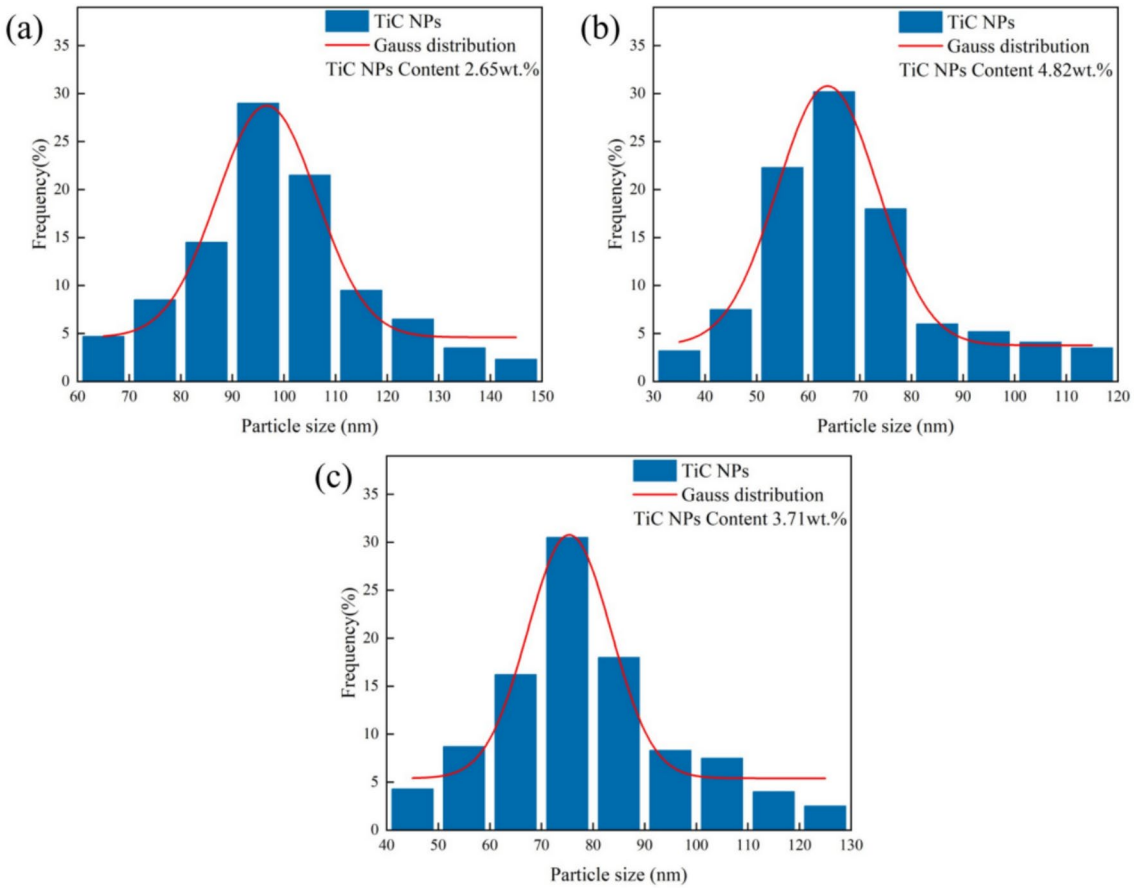

Fig. 7. TiC Ns sizes of Ni-TiC composites deposited at various nozzle angles: (**a**) 30°, (**b**) 45°, and (**c**) 60°

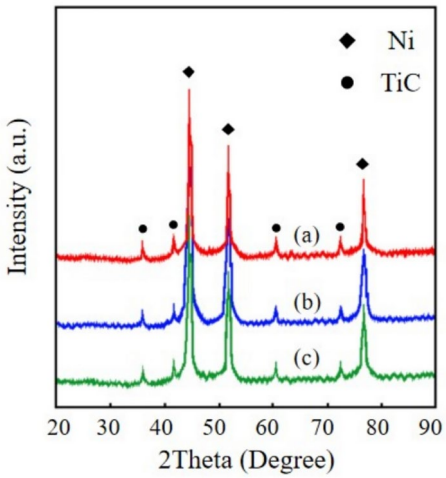

Fig. 8. XRD patterns of Ni-TiC composites produced at various nozzle angles: (**a**) 30°, (**b**) 45°, and (**c**) 60°

were 0.51 μm, 0.22 μm, and 0.37 μm, respectively. These findings are consistent with the conclusions drawn by Dehgahi et al.[25] and Hamed et al.[26].

Abrasion resistance test

Figure 9 illustrates the variation in microhardness values of Ni-TiC composites fabricated at different nozzle angles. As depicted, the microhardness initially increased and subsequently decreased with a rise in the nozzle angle. Specifically, the microhardness value for the Ni-TiC composite prepared at a nozzle angle of 30° was

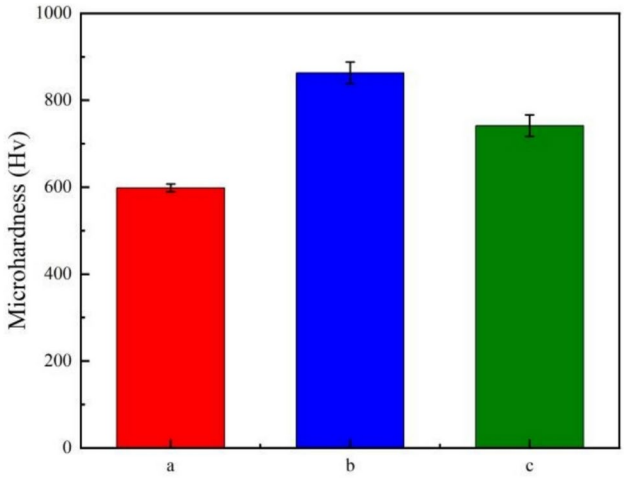

Fig. 9. Microhardness values of Ni-TiC composites produced at various nozzle angles: (**a**) 30°, (**b**) 45°, and (**c**) 60°

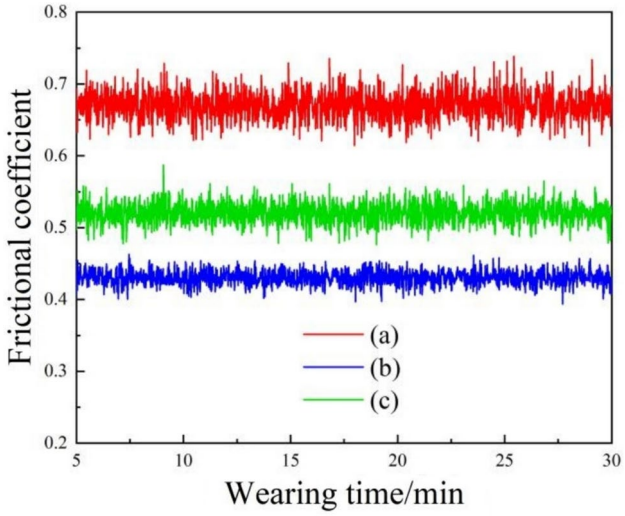

Fig. 10. Friction coefficients of Ni-TiC composites fabricated at various nozzle angles: (**a**) 30°, (**b**) 45°, and (**c**) 60°

measured to be 598.1 Hv. When the nozzle angle was increased to 45°, the microhardness value rose to 863.2 Hv. However, further increasing the nozzle angle to 60° led to a decrease in microhardness to 741.6 Hv.

The nozzle angle significantly influences the microstructure and performance of the composites through variations of jet velocity and spraying pressure during jet electrodepsoition process[27]. At an optimal jet velocity and spraying pressure—achieved at a 45° nozzle angle—the co-deposition rate of Ni^{2+} ions and TiC nanoparticles (NPs) was maximised, resulting in enhanced dispersion hardening and improved microhardness. This high co-deposition rate of Ni^{2+} ions and TiC NPs resulted in strong dispersion hardening, thereby enhancing the microhardness value. In contrast, both lower (30°) and higher (60°) nozzle angles led to suboptimal jet velocities and spraying pressures, reducing the co-deposition rate of Ni^{2+} ions and TiC NPs. At a nozzle angle of 30°, the low jet velocities and spraying pressures generated inferior dispersion hardening. However, the nozzle angle of 60° produced high jet velocities and spraying pressures unfavorable for the co-deposition of Ni^{2+} ions and TiC NPs. This lower deposition efficiency mentioned above resulted in a significant decrease in microhardness for the composites synthesized at these angles.

Figure 10 illustrates the frictional coefficients associated with Ni-TiC composites fabricated at various nozzle angles. Li et al.[28] reported that the size, content, and distribution of NPs significantly influence the frictional coefficient of nickel-based composites. Undoubtedly, a lower frictional coefficient can markedly improve the wear resistance of nickel-based coatings. The agglomeration and uneven distribution of TiC NPs on the coating surface tend to increase the frictional coefficient of the composites. Additionally, the average frictional coefficients for the nozzle angles of 30°, 45°, and 60° Ni-TiC composites were 0.67, 0.43, and 0.52, respectively. The Ni-TiC

composites prepared with a nozzle angle of 45° exhibited a lower average frictional coefficient compared to those made with nozzle angles of 30° and 60°, indicating superior abrasion resistance at this angle.

This phenomenon was attributed to the variations in the size and number of TiC NPs on the surface of Ni-TiC composites produced at different nozzle angles, resulting in significant changes in the frictional coefficient. Li et al.[29] proposed that the low content and agglomerated reinforced phase NPs of composites possessed high frictional coefficient, which was similar to the frictional coefficient of composites fabricated at nozzle angles of 30° and 60°. In contrast, the composites produced at nozzle angle of 45° owned a sufficient and uniform distribution of TiC NPs in the composites, which could effectively reduce plastic deformation of composites under applied load. Therefore, the composites prepared at nozzle angle of 45° had the lowest frictional coefficient, indicating outstanding anti-wear performance.

Figure 11 illustrates the wear mass loss of the Ni-TiC composites fabricated at different nozzle angles. The experimental results demonstrate that the wear mass loss of the Ni-TiC composites initially decreased and subsequently increased with increasing nozzle angle. According to Eq. (3), the wear mass loss of the Ni-TiC composites fabricated at a nozzle angle of 30° was 79.5 mg. When the nozzle angle increased to 45°, the wear mass loss decreased to 37.4 mg. However, when the nozzle angle reached 60°, the wear mass loss increased to 61.2 mg.

The experimental findings can be attributed to the significant influence of high hardness and a low frictional coefficient on the abrasion resistance of the composites. This conclusion aligns with the observations reported by Zhang et al.[30] and Nayana et al.[31]. The variation in jet velocity and spraying pressure of the electrolyte results in an inhomogeneous deposition rate on the cathode surface. Such a deposition rate leads to a loose and coarse microstructure in the composites, characterized by reduced hardness and an increased frictional coefficient, ultimately leading to higher wear mass loss[32]. Conversely, at an optimal nozzle angle of 45°, the composites exhibit a compact and smooth microstructure with a low frictional coefficient and high hardness, which significantly reduces the wear mass loss[33].

The abrasive surface morphologies of the Ni-TiC composites fabricated at various nozzle angles are illustrated in Fig. 12. The images reveal conspicuous pits and grooves on the worn surfaces of the Ni-TiC composites produced at nozzle angles of 30° and 60°. In contrast, only minor scratches and shallow grooves are observed on the worn surface of the Ni-TiC composite manufactured at a nozzle angle of 45°. Analysis of the SEM images indicates that variations in the wear mechanisms account for the differences in surface features among the Ni-TiC composites. Specifically, composites fabricated at nozzle angle of 30° and 60° with low microhardness and small TiC content, leading to sliding abrasion as the predominant wear mechanism[34]. Conversely, numerous NPs exfoliate from composites obtained at nozzle angle of 45° with large TiC content and high microhardness, transitioning the wear mechanism from sliding abrasion to rolling abrasion[35].

The specific data of Ni-TiC composites fabricated at different nozzle angles is listed in Table 3. When the nozzle angle was 30°, the large size of nickel grain (0.51 μm) and low TiC content (2.65 wt%) generated the low microhardness of 598.1 Hv, large frictional coefficient of 0.67 and high worn mass loss of 79.5 mg. By comparison, after nozzle angle increased to 45°, the nickel grain size, frictional coefficient, and worn mass loss of Ni-TiC composites reduced to 0.22, 0.43, and 37.4 mg, while the TiC content and microhardness increased to 4.82 wt% and 863.2 Hv, respectively. However, when the nozzle angle was 60°, the nickel grain size, frictional coefficient, and worn mass loss of Ni-TiC composites increased to 0.37, 0.52, and 61.2 mg, while the TiC content and microhardness decreased to 3.71 wt% and 741.6 Hv, respectively. Therefore, in comparison to the Ni-TiC composites manufactured at nozzle angle of 30° and 60°, the one produced at nozzle angle of 45° had the optimal microstructure and abrasion resistance.

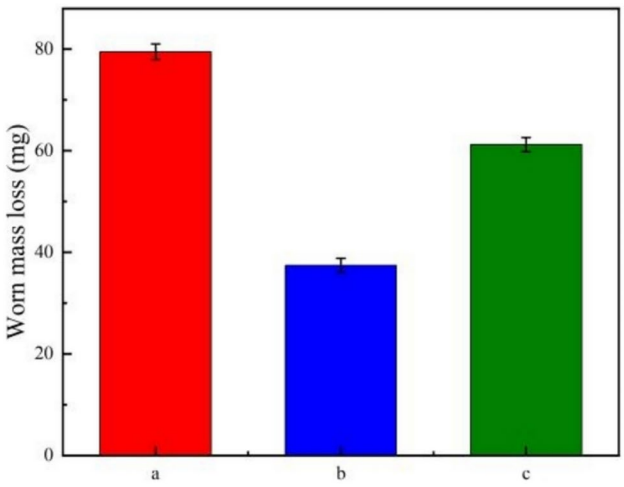

Fig. 11. Worn mass losses of Ni-TiC composites produced at various nozzle angles: (**a**) 30°, (**b**) 45°, and (**c**) 60°

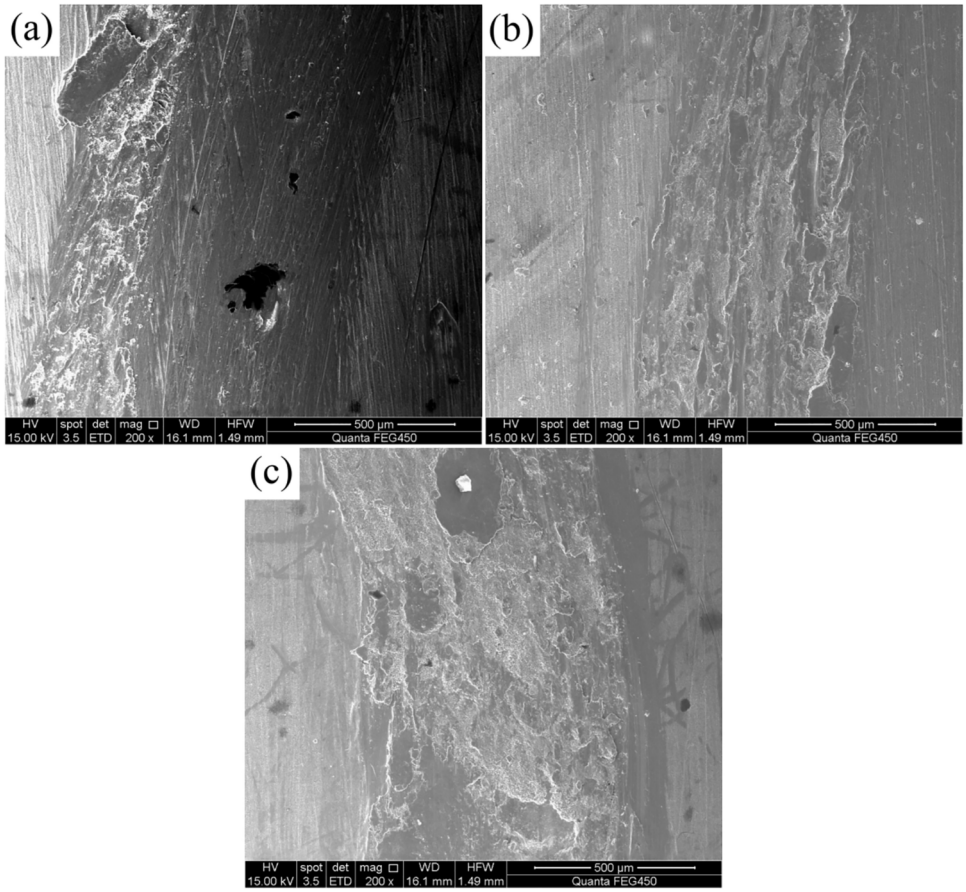

Fig. 12. Abrasive surface morphologies of Ni-TiC composites built at various nozzle angles: (**a**) 30°, (**b**) 45°, and (**c**) 60°

Ni-TiC composites	Ni grain size(µm)	TiC content (wt%)	Microhardness value (Hv)	Frictional coefficient	Worn mass loss (mg)
Obtained at 30° nozzle angle	0.51	2.65	598.1	0.67	79.5
Obtained at 45° nozzle angle	0.22	4.82	863.2	0.43	37.4
Obtained at 60° nozzle angle	0.37	3.71	741.6	0.52	61.2

Table 3. Specific data of Ni-TiC composites obtained at various nozzle angles.

Conclusion

1. At a nozzle angle of 45°, the optimal jet velocity and spraying pressure were determined to be 3.17 m/s and 3.18×10^4 Pa, respectively. This configuration resulted in a compact and flattened surface morphology, with a uniform distribution of TiC NPs emerged on the surface of the Ni-TiC composites. In contrast,when the nozzle angle was set to 30° and 60°, a coarse and uneven surface morphology were observed, characterized by significant agglomeration of TiC NPs on the surface of the composites.
2. The XRD analysis revealed that the diffraction peak intensities of Ni-TiC composites fabricated at a nozzle angle of 45° were lower than those of the composites produced at other nozzle angles, indicating a refinement in grain size. Additionally, the TiN content in the Ni-TiC composites manufactured at 45° was significantly higher compared to those produced at 30° and 60°.
3. The nozzle angle also had a substantial impact on the abrasion performance of the Ni-TiC composites. Specifically, composites fabricated at a nozzle angle of 45°, the Ni-TiC composites exhibited the least wear, with minimal mass loss of 37.4 mg and only minor scratches visible on the surface, demonstrating superior abrasion resistance.

Data availability

The datasets used and/or analysed during the current study available from corresponding author on reasonable request.

Received: 22 January 2025; Accepted: 16 April 2025
Published online: 28 April 2025

References

1. Safavi, M. S. et al. Electrodeposited Ni-Co alloy-particle composite coatings: A comprehensive review. *Surf. Coat. Technol.* **382**, 125153 (2020).
2. Molaei, M. & Atapour, M. Nickel-based coatings as highly active electrocatalysts for hydrogen evolution reaction: A review on electroless plating cost-effective technique. *Sustain. Mater. Technol.* **40**, e00991 (2024).
3. Wu, S. et al. Controllable preparation of metal-based lubrication coatings in extreme environmental applications. *Mater. Des.* **241**, 112922 (2024).
4. Qu, S. W. et al. Diamond particles-reinforced Ni-based composite coating on Ti6Al4V alloy: Microstructure, mechanical, dynamic impact and dry-sliding tribological properties. *Surf. Coat. Technol.* **458**, 129307 (2023).
5. Li, L. Q. et al. Effect of pre-oxidation on the electrochemical corrosion behavior of Ni-based coating reinforced by ceramic particles. *Ceram. Int.* **49**(11), 18095–18103 (2023).
6. Bahrami, F., Amini, R. & Taghvaei, A. H. Microstructure and corrosion behavior of electrodeposited Ni-based nanocomposite coatings reinforced with Ni60Cr10Ta10P16B4 metallic glass particles. *J. Alloys Compd.* **714**, 530–536 (2017).
7. Nyambura, S. M. et al. Synthesis and characterization of Ni-W/Cr_2O_3 nanocomposite coatings using electrochemical deposition technique. *Coatings* **9**(12), 815 (2019).
8. Shao, W. et al. Mechanical and anti-corrosion properties of TiO_2 nanoparticle reinforced Ni coating by electrodeposition. *J. Electrochem. Soc.* **159**(11), D671–D676 (2012).
9. Qu, N. S., Qian, W. H., Hu, X. Y. & Zhu, Z. W. Fabrication of Ni-CeO_2 nanocomposite coatings synthesised via a modified sediment co-deposition process. *Int. J. Electrochem. Sci.* **8**(9), 11564–11577 (2013).
10. Yang, N. et al. Physicochemical state classification of heat-treated TC4 samples based on laser-induced breakdown spectroscopy (LIBS). *At. Spectrosc.* **45**(4), 324–335 (2024).
11. Bai, C. Y. et al. Effect of different Mg2Si concentrations on the wear properties and microstructure of Mg2Si/Al-5wt.% Cu composites. *Int. J. Metalcast.* **19**, 1–13 (2024).
12. Wang, F. B. et al. Effect of electropulsing treatment on the microstructure and mechanical properties of Ti6Al4V alloy processed by a hybrid method of directed energy deposition and layer-by-layer ultrasonic impact peening. *Mater. Sci. Eng. A* **908**, 146774 (2024).
13. Gyawali, G., Cho, S. H., Woo, D. J. & Lee, S. W. Pulse electrodeposition and characterisation of Ni-SiC composite coatings in presence of ultrasound. *Trans. Inst. Met. Finish.* **90**(5), 274–280 (2012).
14. Yang, M. L., Xu, J. L., Huang, J., Zhang, L. W. & Luo, J. M. Wear resistance of N-doped CoCrFeNiMn high entropy alloy coating on the Ti-6Al-4V alloy. *J. Therm. Spray Technol.* **33**(7), 2408–2418 (2024).
15. Hu, X. Y. & Qu, N. S. Improved corrosion resistance of Ni-Co coatings prepared by electrodeposition with large centrifugal acceleration. *J. Mater. Eng. Perform.* **28**(4), 2104–2114 (2019).
16. Ren, A. H., Kang, M. & Fu, X. Q. Tribological behaviour of Ni/WC-MoS_2 composite coatings prepared by jet electrodeposition with different nano-MoS_2 doping concentrations. *Eng. Fail. Anal.* **143**, 106934 (2023).
17. Meng, Q. J. et al. Microstructure and performance optimization of laser cladding nano-TiC modified nickel-based alloy coatings. *Surf. Coat. Technol.* **479**, 130583 (2024).
18. Wu, W. P. et al. The influence of Re content on microstructure, grain size, microhardness and abrasion resistance of electrodeposited Ni-Re alloy coatings. *Wear* **512–513**, 204551 (2023).
19. Song, Z. Y. et al. Graphene nanosheet as a new particle dispersant for the jet-electrodeposition of high-performance Ni-P-WC composite coatings. *Surf. Coat. Technol.* **425**, 127740 (2021).
20. Wang, C., Shen, L. D., Qiu, M. B., Tian, Z. J. & Jiang, W. Characterizations of Ni-CeO_2 nanocomposite coating by interlaced jet electrodeposition. *J. Alloys Compd.* **727**, 269–277 (2017).
21. Li, H. G. et al. Fabrication and characterization of Ni-Co-TiN/CeO_2 composite coating by ultrasonic vibration-assisted jet electrodeposition. *Colloids Surf. A* **687**, 133526 (2024).
22. Ren, N. N., Shen, M. Q., Ma, W. K., Duan, S. L. & Ding, L. Y. Optimization of the nozzle structure for enhanced wear resistance of Ni-P-ZrO2 composite coating prepared by jet electrodeposition. *Int. J. Electrochem. Sci.* **15**(9), 9154–9167 (2020).
23. Bakhit, B. & Akbari, A. Synthesis and characterization of Ni-Co/SiC nanocomposite coatings using sediment co-deposition technique. *J. Alloys Compd.* **560**, 92–104 (2013).
24. Pingale, A. D., Belgamwar, S. U. & Rathore, J. S. Synthesis and characterization of Cu-Ni/Gr nanocomposite coatings by electro-co-deposition method: effect of current density. *Bull. Mater. Sci.* **43**(1), 66 (2020).
25. Dehgahi, S., Amini, R. & Alizadeh, M. Corrosion, passivation and wear behaviors of electrodeposited Ni-Al_2O_3-SiC nanocomposite coatings. *Surf. Coat. Technol.* **304**, 502–511 (2016).
26. Hamed, A. E., Vaezi, M. R., Nikzad, L., Yazdani, B. & Sadrnezhaad, S. K. Influence of SiC nanoparticles and saccharin on the structure and properties of electrodeposited Ni-Fe/SiC nanocomposite coatings. *J. Alloys Compd.* **484**(1–2), 540–544 (2009).
27. Cui, W., Wang, K., Xia, F. F. & Wang, P. Simulation and Characterization of Ni-doped SiC nanocoatings prepared by jet electrodeposition. *Ceram. Int.* **44**(5), 5500–5505 (2018).
28. Li, C. Y., Xia, F. F., Ma, C. Y. & Li, Q. Research on the corrosion behavior of Ni-SiC nanocoating prepared using a jet electrodeposition technique. *J. Mater. Eng. Perform.* **30**(8), 6336–6344 (2021).
29. Li, B. S. et al. Ultrasonic-assisted electrodeposition of Ni/diamond composite coatings and its structure and electrochemical properties. *Ultrason. Sonochem.* **73**, 105475 (2021).
30. Zhang, X. S. et al. Effect of microstructure and micromechanics on wear/wear-corrosion mechanism of laser-repaired Ni-WC coating. *Eng. Fail. Anal.* **162**, 108337 (2024).
31. Nayana, K. O., Ranganatha, S., Shubha, H. N. & Pandurangappa, M. Effect of sodium lauryl sulphate on microstructure, corrosion resistance and microhardness of electrodeposition of Ni-Co_3O_4 composite coatings. *Trans. Nonferrous Metals Soc. China* **29**(11), 2371–2383 (2019).
32. Demir, M., Kanca, E. & Karahan, I. S. H. Characterization of electrodeposited Ni-Cr/hBN composite coatings. *J. Alloys Compd.* **844**, 155511 (2020).
33. Wong, M. S., Hsiao, G. Y. & Yang, S. Y. Preparation and characterization of AlN/ZrN and AlN/TiN nanolaminate coatings. *Surf. Coat. Technol.* **133–134**, 160–165 (2000).
34. Hong, S. et al. Influences of sand concentration and flow velocity on hydro-abrasive erosion behaviors of HVOF sprayed Cr_3C_2-NiCr and WC-Cr_3C_2-Ni coatings. *J. Market. Res.* **21**, 1507–1518 (2022).
35. Xia, F. F., Li, C. Y., Ma, C. Y., Li, Q. & Xing, H. Y. Effect of pulse current density on microstructure and wear property of Ni-TiN nanocoatings deposited via pulse electrodeposition. *Appl. Surf. Sci.* **538**, 148139 (2021).

Acknowledgements
This work has been supported by the Intelligent manufacturing critical technique research and industrialization of high quality rod stock (Granted No. 2023XQ009) and the Natural science foundation of Heilongjiang province (Granted No. LH2023A002).

Author contributions
M.C. and C.L. wrote the main manuscript text, X.G. and F.Z. conducted the experiment, W.L. and B.W. prepared figures 1–12. All authors reviewed the manuscript and M.C. and C.L. had equal contribution in the manuscript.

Declarations

Competing interests
The authors declare no competing interests.

Additional information
Correspondence and requests for materials should be addressed to C.L., B.W., X.G. or W.L.

Reprints and permissions information is available at www.nature.com/reprints.

Publisher's note Springer Nature remains neutral with regard to jurisdictional claims in published maps and institutional affiliations.